TDR of Diagnostic Activities in SPARC Project

A.Doria, G.P. Gallerano, L.Giannessi, E.Giovenale
ENEA, UTS FIS, Via E. Fermi 45 Frascati

General layout for optical diagnostics (1st year)

The general layout for the optical diagnostics is reported in Fig. 1. At the end of any undulator section a diagnostic chamber is placed by means of which the FEL radiation is extracted and transported to a measurement station located at the end of the overall FEL device. The radiation will be transported through a 2 inch light pipe that can be evacuated or filled with dry air (or nitrogen) in order to reduce the absorption in air both at the fundamental frequency and at all the UV harmonics.

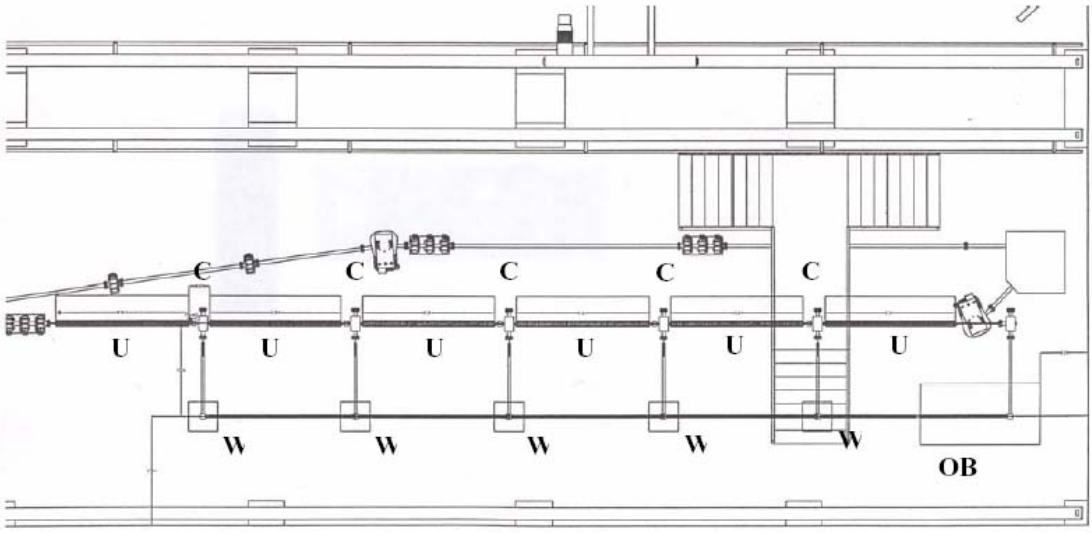

Fig. 1 Experimental layout of the experimental area: U indicates the magnetic undulator section; C is the diagnostic chamber; W is the breadboard of 750 mm x 750 mm for the analysis of the radiation extracted from any section U. At the end of the last section an optical table (OB) of 1200mm x 2400 mm is placed, for the analysis of the radiation coming from each W.

A further light pipe will realised to transport the FEL radiation to a "Diagnostic Hall" that is located above the SPARC bunker (see Fig. 2). This "Diagnostic Hall" is separated and protected with concrete shields and thus has the advantage to let operators to work protected from ionizing radiation. It will be equipped with two optical tables, and the necessary instrumentation, for all the measurements of the spectral and temporal characteristics of the FEL radiation and, in case, for some preliminary applicative tests.

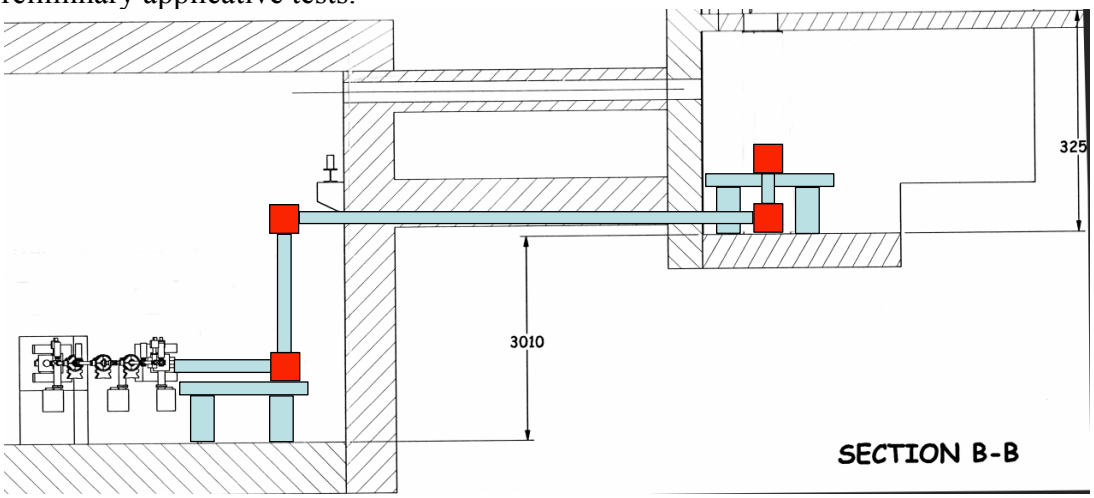

Fig.2 Layout of the light pipe for the radiation transport to the "Diagnostic Hall"

Undulator Vacuum Chamber (1st year)

The overall dimensions that the vacuum chamber to be placed within the six undulator sections must primarily satisfy the requirements about the gap between the two trains of magnets. The nominal gap has been, in fact, fixed to a value of 9.5 mm for an operation at a wavelength of 500 nm. The external vertical size, within the gap, has been fixed in 8 mm to allow a suitable tolerance to align the chamber and to set properly the correct gap value (see Fig.1). Eventual smaller values of gap required by experiments within SPARC project will require the realisation of a new vacuum chamber, but the costs will not influence very much the overall budget of the project.

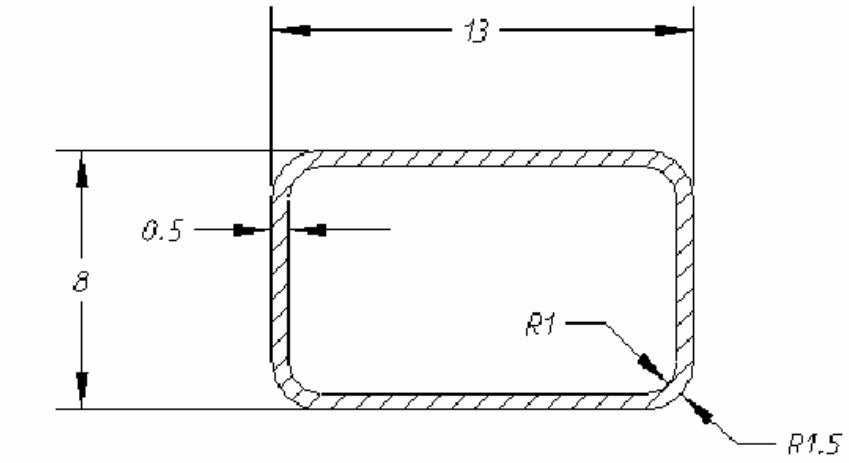

Fig. 1 Transverse section of the undulator vacuum chamber (quotes are expressed in mm).

As far as the second transverse dimension, orthogonal to the magnetic field, is concerned, we have decided for a dimension of 13 mm that guarantees an adequate stiffness to the chamber, as we will discuss later, and allows an easy way to provide some lateral mechanical support systems (see Fig. 2). From these considerations the vacuum chamber will be realised by means of six pipe sections with rounded corners and thickness of 0.5 mm. Any section is delivered with a length of 2500 mm and is made of non-magnetic stainless steel AISI 316L.

Fig. 2Global view of the undulator vacuum chamber including supports and flanges.

The high vacuum flanges will be soldered at the ends of any pipe section, while during the first tests it will be considered the possibility to insert some electron position monitors from the side walls of the chamber.

As far as the vacuum is concerned we are considering a vacuum limit of $P=10^{-7}$ mbar at the centre of each 2.5 m pipe section. Such a pressure value can be obtained with a pumping group realised with:

- Pre vacuum: Dry multistage rough pump of 28 m^3/h
- High vacuum: turbo-molecular pump of 70 l/s.
- High vacuum: regime operation with an ion pump of 200 l/s having no vibrations.

The vacuum measurements will be realised inside the diagnostic vacuum chamber that will be located at the end of any undulator section, as described below. The expected time to reach the final pressure of $P=10^{-7}$ mbar is about 12 hours. For maintenance purposes any section will be separated by means of high vacuum VAT electro-valves. Any pumping group will be equipped with its own vacuum valve, power supply unit and control, low and high vacuum gauges, filters, PC-based computers with proper software codes realised in LabView for the automation of the process and for the data control. A prototype of an undulator channel section will be tested in order to verify the pressure fall along the pipe and the roughness of the surface in order to run the proper simulations on the possible wake-field effects.

Undulator Vacuum Chamber (2nd year)

The vacuum system, to be realised, requires that some experimental requirements may be respected, such as the pressure to be maintained in proximity of the photo-cathode surface, the dimensions of the undulator vacuum chamber, the connections with external diagnostics, located under vacuum or in air. Such constrains force for an accurate design study of the vacuum system in order to fulfil the operating FEL parameters.

The hypothesis of setting a stable but differential vacuum among the different sections of the experimental layout is pursuable, mainly due to the high impedance of the undulator vacuum chamber sections. A difficulty may arise by the overall complexity of the system where we shall place many different pumping systems all linked one to each other. To overcome these problems and to prepare an adequate vacuum project we have acquired the VacSim software that simulates complex vacuum systems. Such software is based on the same, but implemented, algorithms on the electronic systems simulator SPICE, and once given the main systems parameters as input it can give the pressure data and the gradient values in any system section.

In order to test the behaviour of the designed system, an experiment has been set up to test a typical section of the vacuum system: a section of the undulator pipe (1.2 meters long, 1.2x0.8 cm2 section) has been mounted to be evacuated by means of a 68 l/sec turbo-molecular pump (Varian V70LP), backed by a dry scroll pump capable of 82 l/min (Varian SH-100). The system was also connected to a 50 l/s Ion pump (Varian VACION plus 55). Asymptotic vacuum values were measured on both sides of the pipe, measuring the vacuum level near the pumps on one side, and the level on the other side of the pipe, to see the effect of the impedance. A picture of the layout of the test experiment is reported in Fig. 1.

The software is VACSIM MULTI, by SOFTSIM (UK), and makes use of the electronic circuit simulator SPICE libraries making use of the one to one correspondence between vacuum and electronic circuit parameters.

The software allows to define the main components of the circuit and to build up easily a system design, performing a complete simulation on it.

Fig.1 Picture of the vacuum test experiment

In order to test the software we decided to compare the real performances of the simple system we tested to the simulations obtained through Vacsim. The first step was the definition of the parameters of the vacuum components present in the system.

The VACSIM software allows defining the vacuum performances of each component included in the scheme reported in Fig. 2:

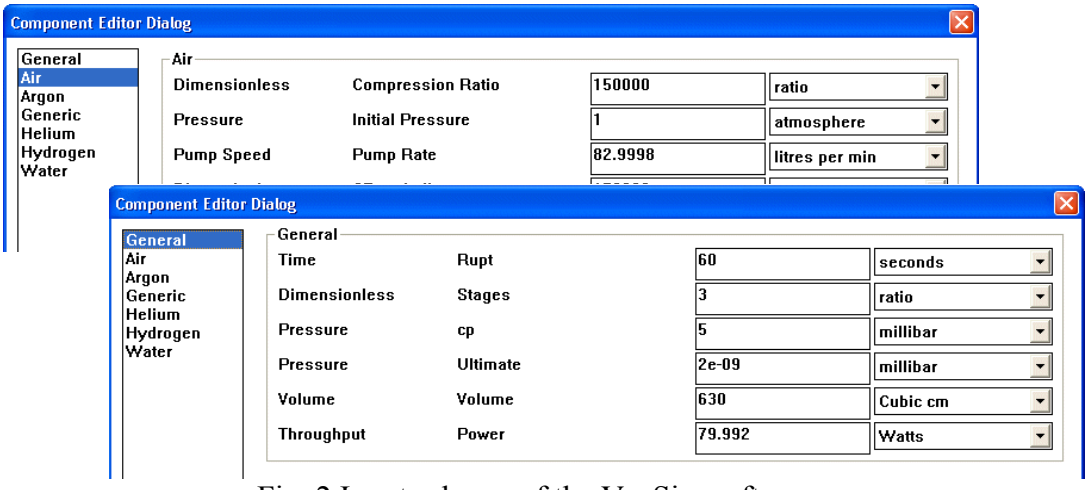

Fig. 2 Input scheme of the VacSim software.

Once the components have been correctly parameterised, including pumps, volumes, impedances, out gassing and leaks, we built a design for the vacuum system as reported in the sketch of Fig. 3:

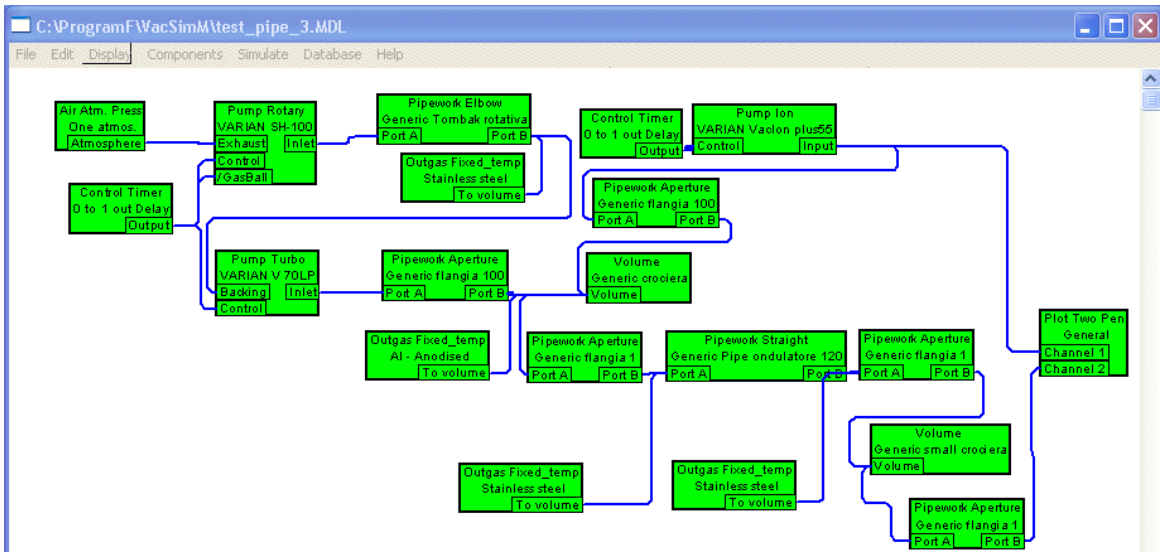

Fig. 3 Sketch of the design vacuum system in the VacSim software.

Simulation results are reported in the graph below (see Fig. 4). The asymptotic value of the vacuum is not far from the experimental value (about 10^{-5} mbar), but in our experiment this value was reached in a longer time. The limit value for vacuum, near the pumps, is similar to the one experimentally observed.

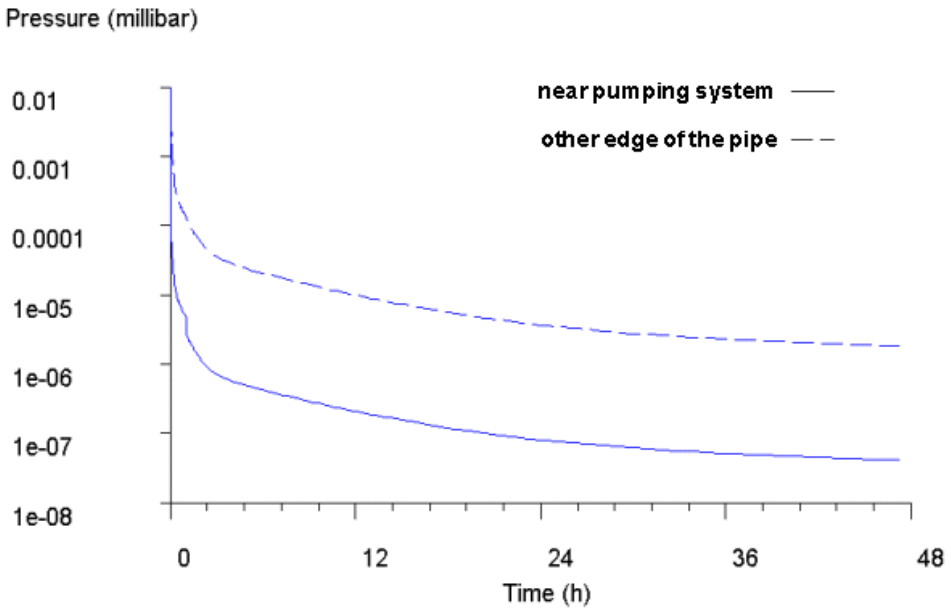

Fig. 4 Graph of the simulation without baking.

Simulation shows that a limit vacuum just below 10^{-5} mbar can be reached with a single TM pump pumping through the pipe impedance. Vacuum difference between the two edges is about a factor 50. Simulations result to be closer to the experimentally verified behaviour if the out gassing rate of the components is set to a higher value. This means that probably we underestimated the out gassing rate of the copper pipe, and that, due to the high impedance of the system, this results in too long a time to reach the limit vacuum.

We then decided to “bake” the pipe in order to clean it up and we repeated the experimental measurements. After baking, the simulation is much closer to the experimental behaviour.

Finally we checked if the system, once reached an adequate value of the pressure, can be retained at the required vacuum level by the ion pump only.

Simulations have been performed, together with experimental tests, and both gave positive results. The shutdown time of the turbo molecular pump can be easily identified in the graph below (see Fig. 5).

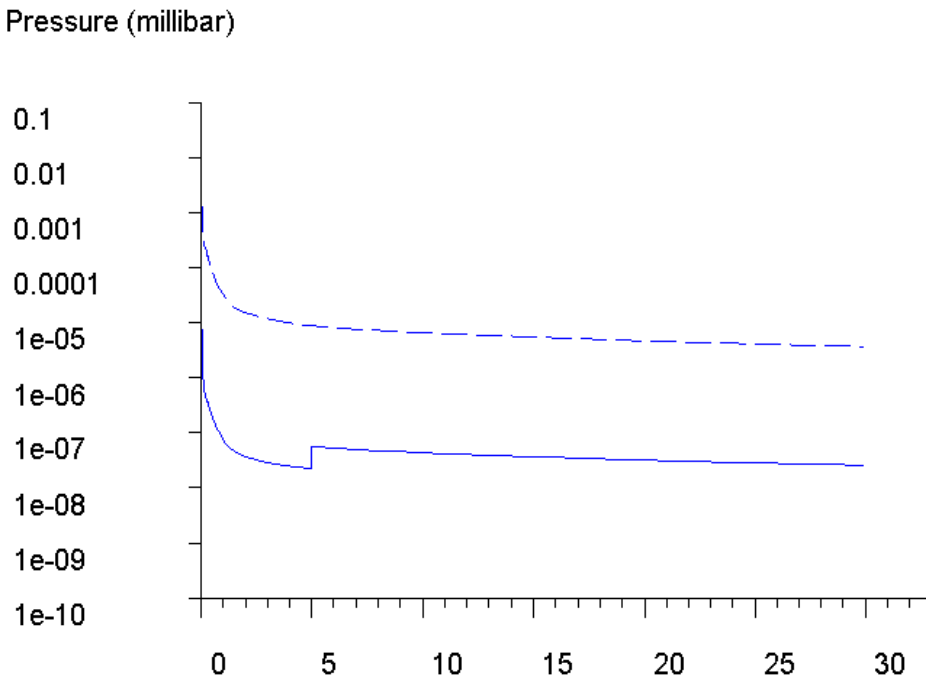

Fig. 5 Fig. 4 Graph of the simulation after the baking.

Operation at the obtained vacuum level should not affect FEL operation: the amount of air molecules in the pipe is equivalent to an aluminium foil with thickness well below 1 Angstrom.

Radiation propagation of fundamentals and harmonics through gas and solids. (2nd year)

The aim of the SPARC project is to generate radiation at a wavelength of 500 nm by means of SASE mechanism. The higher harmonics of this fundamental will be 170 nm for the third and 100 nm for the fifth respectively. Moreover in the seeding experiment is in program to extend the harmonic emission down to the EUV range, i.e. toward 30 nm. This wide frequency tunability introduces problems in coupling the radiation out from the FEL transport channel; this is mainly due to the different attenuation coefficients for the vacuum windows and the air at the different wavelengths.

One of the problems to face while projecting the SPARC diagnostics is to find the best technique to couple the radiation out from the diagnostic chambers that are located between the different undulator sections. The way to couple the radiation is the use of windows that must have a wide spectral transmission range for a thickness sufficient to sustain the differential pressure between the bunker pressure and the vacuum in the transport channel. Moreover, in order to minimize the reflection effects, the windows will be placed at the Brewster angle, but this angle, being related to the refractive index, is a direct function of the wavelength.

The material that present a better transparency in the EUV spectral region is the Lithium Fluoride (LiF) for which a transmittance has been measured down to 120 nm (see Fig. 1).

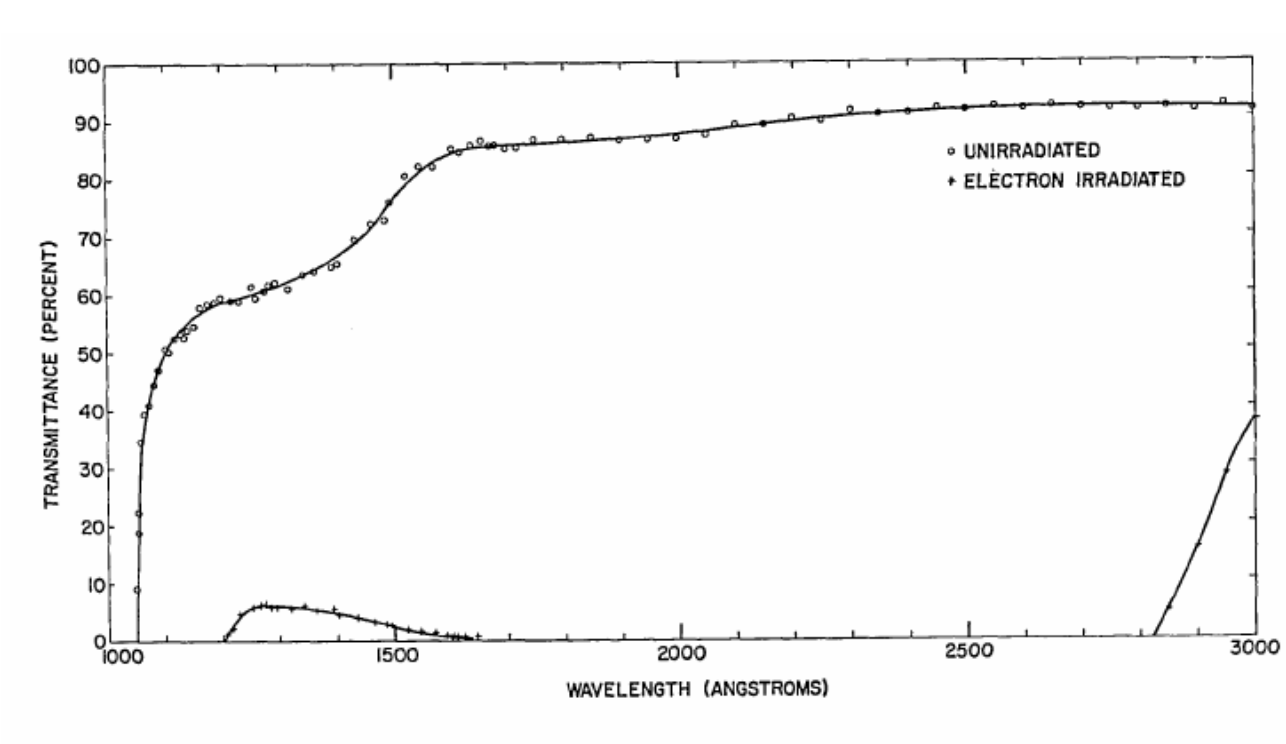

Fig.1 UV Transmittance of a LiF window with a thickness of 2 mm.

As can be seen observing Fig. 1 the transmittance is quite constant, between 85% and 90%, at wavelengths longer than 160 nm and up to 300 nm, but it can be extended up to the near infrared. In the range between 110 nm and 150 nm an absorption band reduces the transmittance to 60%-

70%. Below 120 nm the transmittance falls down due to photon absorption of the core electrons both in the Lithium and Fluorine atoms. Other materials, like MgF_2, CaF_2, $BaF_2$and SiO_2 show transmittance behaviours similar to Fig. 1, where the rapid fall is shifted toward longer wavelengths.

The refractive index behaviour, as a function of wavelength, is important for the evaluation of the reflection coefficient and of the Brewster angle ($\tan(\theta_B)=n_2/n_1$). In Fig. 2 the behaviour of *n* is reported for the LiF material, in the spectral range 120 nm-280 nm. For longer wavelengths, up to about 2000 nm the value remains about fixed around *n=1.4*.

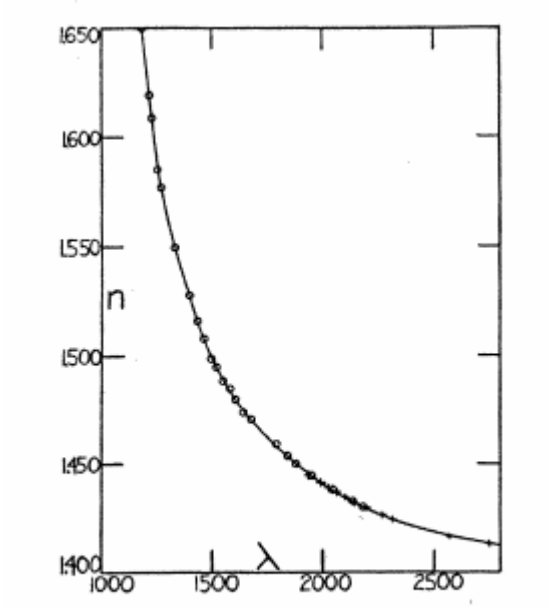

Fig.2 Index of refraction for the LiF in the UV range.

This behaviour ensures a small variation of the Brewster angle for the different harmonics allowing a good control of the reflected component.

Downstream the window the radiation will be transported in the free space before arriving to the experimental area for the temporal, spatial, spectral and amplitude analysis. During this transport the radiation will be attenuated by the air, but different there are absorption mechanism responsible at the different wavelengths. The water vapour in the air is responsible for the absorption in the visible and in the infrared, but allows a transmittance higher than 40% at wavelengths shorter than 600 nm.

At much higher frequencies the EUV photons interact with electronic levels of the atoms, i.e. in the case of the air, mainly with the nitrogen. The absorption coefficients for such atoms, expressed as cm^2/g are reported in Fig. 4 as a function of the photon energy. As can be seen such coefficients for Nitrogen, Oxygen and Aluminium are numerically similar. It can also be noted that the absorption peak is obtained for photons of 10 eV, i.e. for radiation of about 100 nm of wavelengths. Higher energetic photons experience smaller attenuation; thus if we want to evaluate the air transparency at 100 nm we should use the following expression:

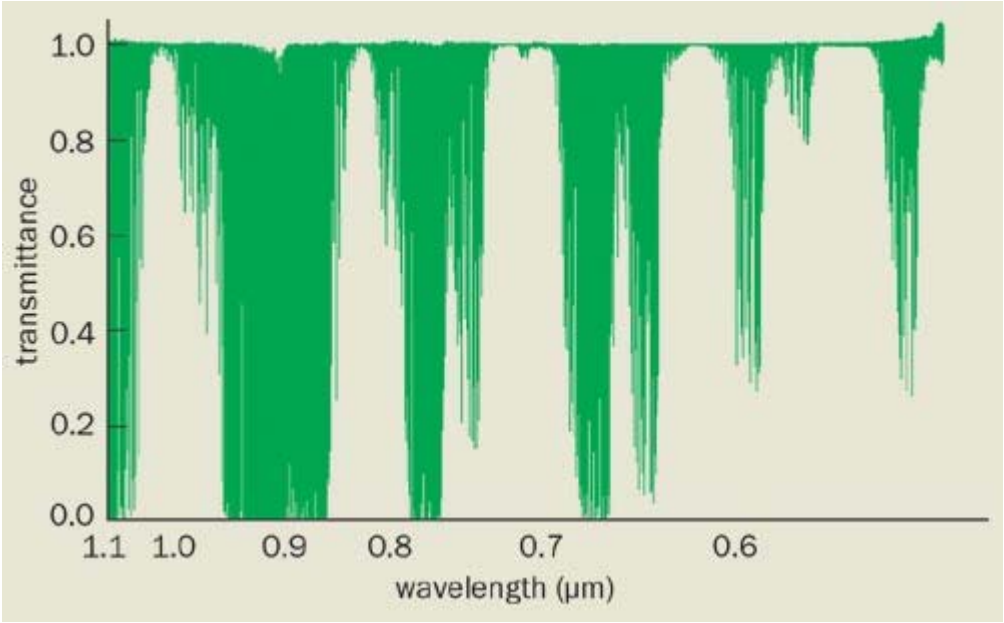

Fig.3 Water vapour transmission in the visible and infrared.

$$T(P,d) = \exp(-\rho(P)\mu d) \tag{1}$$

where $\rho(P)$ represents the air density as a function of the pressure, μ is the attenuation coefficient and d represents the air thickness crossed by the radiation. In order to simplify the calculations we can obtain the $\rho(P)$ behaviour from the perfect gas law, and the result is:

$$\rho(P) = n\text{AMU}\frac{P}{k_B T} \tag{2}$$

where n indicates the atomic gas number, AMU=1.6605402 10^{-27} Kg is the atomic mass unit, k_B is the Boltzman constant and T is the temperature. Evaluating the expression (2), under the hypothesis of a medium composed by a bi-atomic nitrogen only ($n=2*15.007$) at a pressure $P=1$ *atm* and a temperature $T=300$ *K*, we obtain a density for the gas of $\rho=1.22$ *Kg/m*^{3}. By substituting this value into the expression (1) and reading the attenuation coefficient value for the nitrogen from Fig.4 ($\mu=2\ 10^5$ *cm*^{2}*/g*), we obtain the behaviour of the radiation transmission in air, as a function of the pressure, for a wavelength of 100 nm. Such behaviour is reported in Fig. 5 where three different curves are reported each one corresponding to a different path length of air crossed, i.e. *1 cm, 10 cm* and *1* metre.

From a proper analysis of Fig. 5 it can be observed that, at a pressure $P=10^{-2}$ *torr*, it is possible to cross, with a low attenuation of about 70%, 1 metre of air. Higher values of pressure are recommended only for shorter paths.

The conclusions of this short study are that if we want to analyse the fifth harmonic of the SPARC source we must realise a radiation transport channel under vacuum, with pressure values not higher than 10^{-2} *torr*. If we consider that the electron beam propagates together with the generated SASE radiation in a vacuum chamber under pressure values of the order of 10^{-6}–10^{-7} *torr*

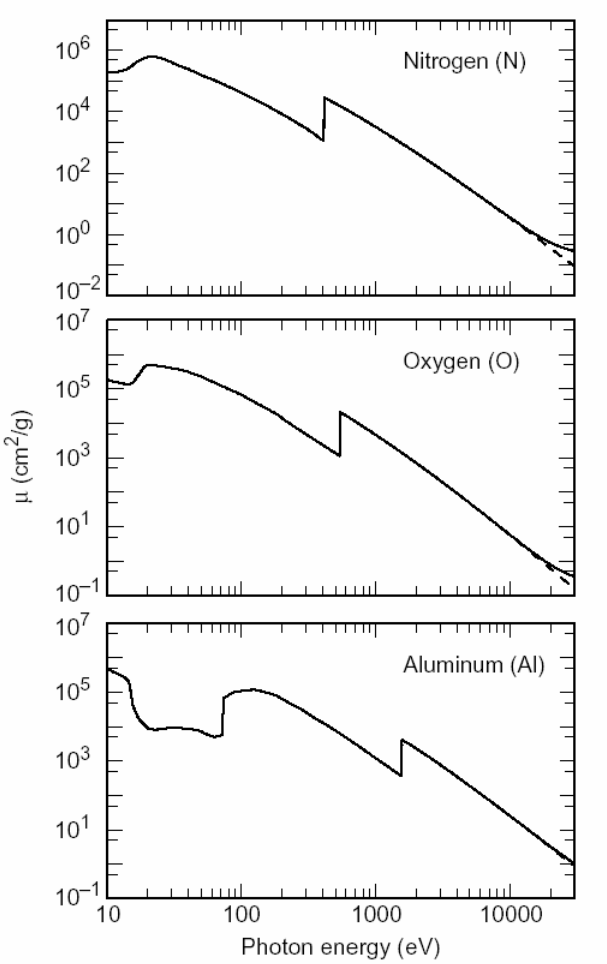

Fig.4 Attenuation coefficient, in the X-ray region, for Nitrogen, Oxygen and Aluminium.

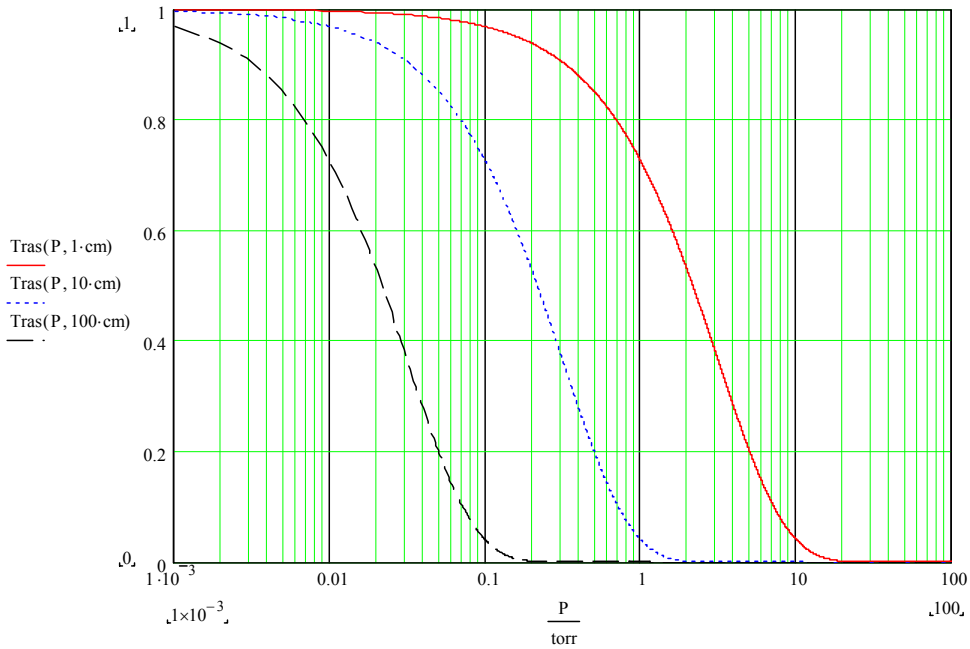

Fig.5 Air transmission, as a function of pressure, at a wavelength of 100 nm.

we can consider two possible solutions for the diagnostics of the radiation and its harmonics. The first consists in having a single value of pressure inside the vacuum transport pipes that must be of the order of $10^{-6} - 10^{-7}$ *torr,* as the electron gun limitations impose. The second solution requires a

differential vacuum between the undulator chamber and the radiation transport pipe. The separation between these two different pressure values can be done with a LiF window that, as previously reported, is the material with a wider spectral transmission range. Moreover due to the fact that this window is required to maintain a differential pressure of 10^{-2} *torr*, it could be realised with small thickness values, as we shall discuss further on. In Fig. 6 we have schematically reported the two different solutions.

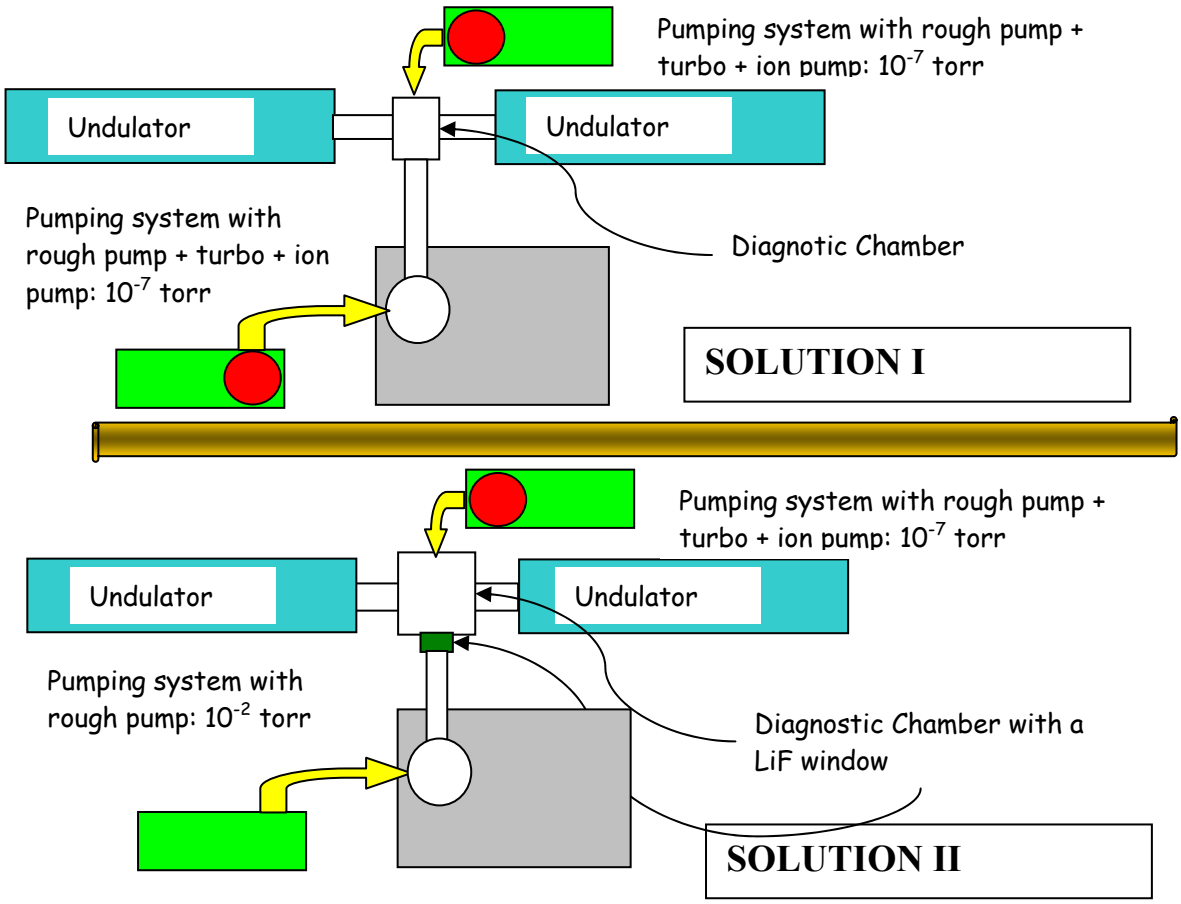

Fig.6 Schematic layouts of the two different solutions for the SPARC SASE radiation transport.

The first layout requires a higher number of pumping systems for the high vacuum (like Turbo pumps with dry back-pumping devices and ion pumps) in order to avoid pressure gradients toward the electron transport channel with a possible damage for the electron gun. The second layout requires only a simple rough-pumping system to evacuate the radiation transport line, but the presence of a window, although made of LiF, limits the spectral range of operation of the diagnostic system.

We can now evaluate the thickness of the windows in case we decide to adopt the second solution. The windows undergo to a constant force due to the difference of pressure between the diagnostic chamber and the radiation transport pipe. The equation that regulates the ratio thickness/ diameter of the window, as a function of the differential pressure applied, before the elasticity limit could be reached is in the following reported. The overcoming of this limit can generate plastic deformations on the window such to modify the optical properties of the crystal and, sometimes, such to make a crack possible in the window itself.

$$\frac{t}{D} = \sqrt{\frac{SF * K}{4} \frac{P}{Fa}} \qquad (3)$$

In the equation (3) *SF* indicates a safety factor that, conventionally is set to a value of 4, *Fa* correspond to the value for the elasticity limit that for the LiF crystal is: $Fa=1.58\ 10^3\ psi$; finally *K* corresponds to a constant related to the geometry of the fixing system of the window: in our case *K=0.75*. In Fig 7 the behaviour of the equation (3) is reported for the LiF in the same range of pressure utilised for Fig. 5.

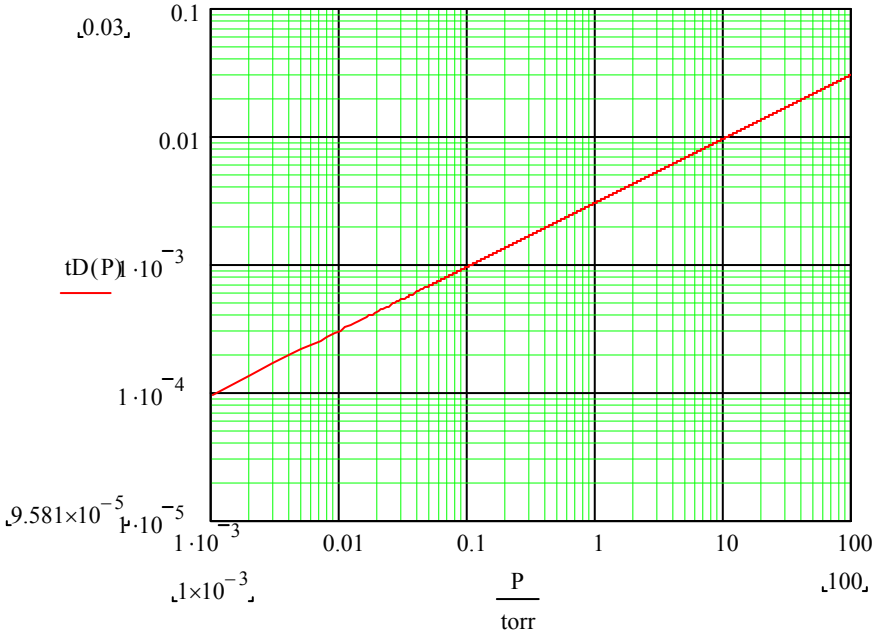

Fig.7 LiF crystal crack limit: ratio between thickness and diameter vs. pressure.

As can be observed in Fig. 7 for a pressure value of $P=10^{-2}\ torr$ we can obtain a ratio between the thickness and the diameter of the window of $2\ 10^{-4}$, this means that for windows having a diameter of 25 mm (about 1 inch) we are allowed to have thicknesses of few microns that can guarantee an extremely high transparency. In the worst case of a pressure value of one atmosphere (that correspond to have the radiation transport pipe in air) the thickness for a LiF window of 25 mm in diameter would be 2mm; this means that Figure 1 reports the transmittance of a LiF window of 25 mm in diameter capable to withstood a pressure of one atmosphere.

Diagnostic Chamber (2nd year)

The project of the diagnostic chamber is mainly based on the definition of the available free space between two consecutive undulator sections. The technical drawings reported in Fig.1 and Fig.2 indicate how the chambers could be realised under the present hypothesis. Inside the chamber are present two different vertical actuation systems, with three steps, capable to host different optical systems. The vertical movement will be realised by means of motorised linear stages, with no rotational actuation, together with linear encoders with closed-loop control. The reason is that the position of the optics must be determined with a very high precision and repeatability of the order of 10-20 μm. Such necessity is related to the fact that electron beam misalignments higher than these values may dramatically alter, the non linear SASE process, preventing to obtain saturation within spaces designed for the SPARC project. Observing again Fig.1 it can be seen that in order to suppress the Wake-Field effects we had to introduce some channel sections that can guarantee the geometrical and electrical conductivity. In so doing the impedance mismatch, experienced by the electrons, is reduced to a minimum, i.e. only in the regions of the space where are located the mirrors and the fluorescent targets for the electrons. The linear stage actuations must be independent and the resulting consequence is that it was necessary to consider two different channel sections, one at the entrance and the other at the exit, of each optical element.

The problems that are still open, and that prevent us to definitively launch the project are two: the first is related to the final projects for the focusing quadrupole and for the Phase-Shifter. These projects are important in order to set the ultimate longitudinal available space that will allow us to project, in details, the single components, like, for instance, the longitudinal channel sections which design must be vary accurate.

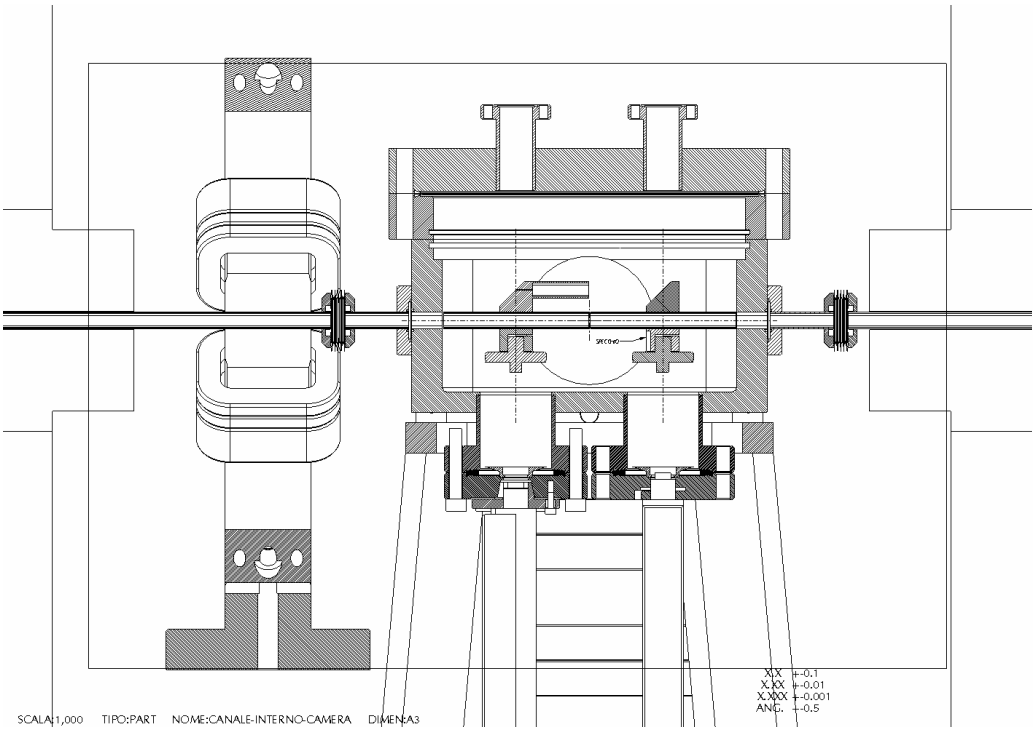

Fig.1 Drawing of the diagnostic vacuum chamber together with the focusing quadrupole.

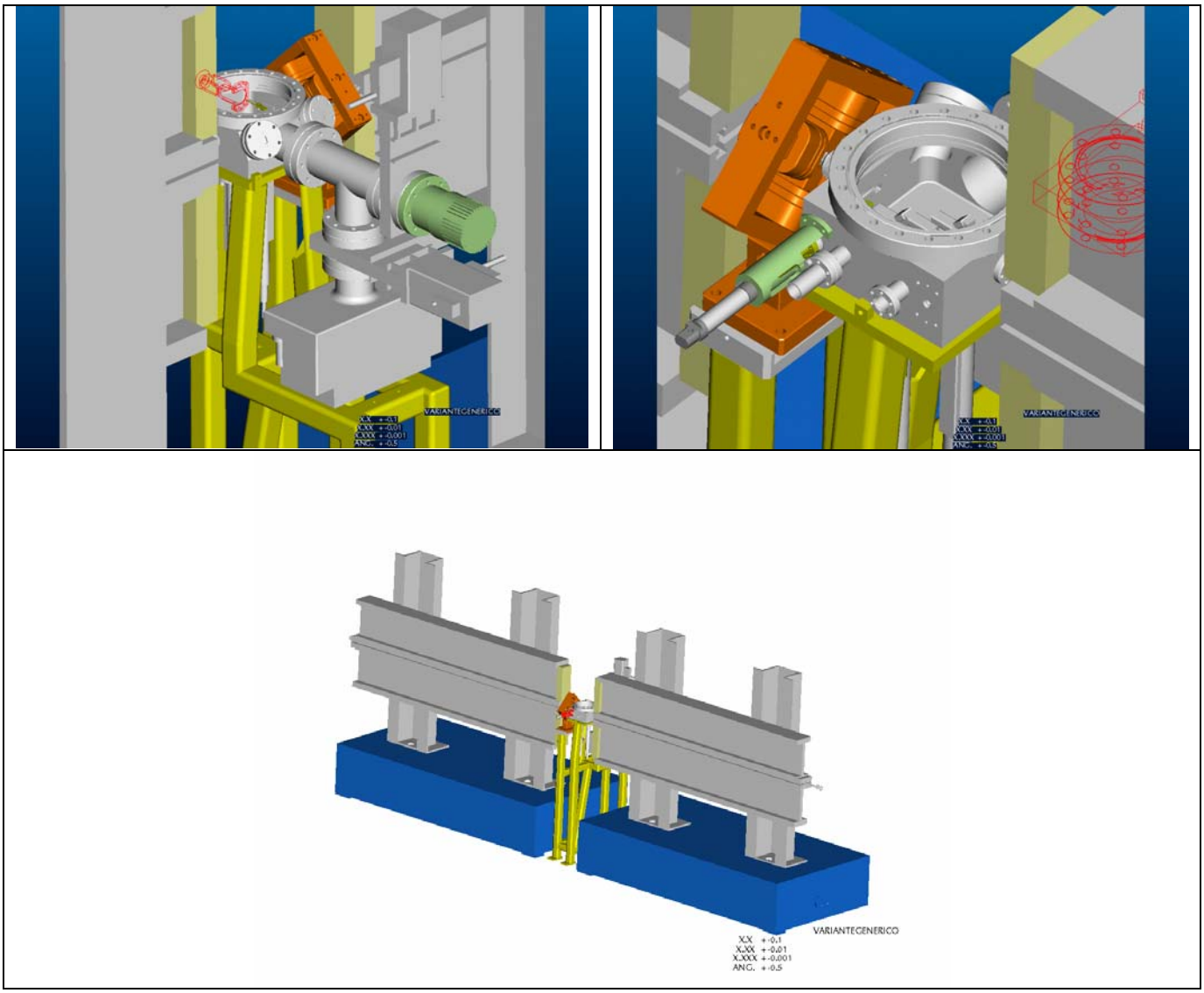

Fig. 2 Drawings of the diagnostic chamber between the two undulator sections.

The second problem is related to the project of the Beam Position Monitor (BPM) for which two ways are under investigation; the first, much traditional, requires the use of four electrodes sensitive to the electric field of the electron beam. Downstream the sensors proper acquisition electronics (like for instance the MX-BPM module from Bergoz) can supply the electron bunch distances from the electrodes, and thus the transverse position of the bunch. The second possible way, not well experimentally established, consists in the use of an optical fibre that, due to the Faraday effect, can induce a polarisation rotation, to the propagating radiation, generated by the electric field of the electron beam. This rotation is proportional to the fibre length and to the electric field amplitude.

Magnetic Measurements (2nd year)

The device for the magnetic map measurements of the undulator sections has been realised about twenty years ago, is called coordinatometer and is presently under refurbishment. Two are the main reasons for such a refurbishment: the first is related to the necessity of measuring magnetic maps with a resolution higher respect to those realised in the past, for the ENEA FEL experiments in the Infrared, sub-millimetre and millimetre spectral range. The SPARC project, in fact, is designed in order to have relative magnetic errors not higher than 0.1% ($(\Delta B/B<10^{-3})$); at the same time also the error in the period length must be kept within a value of 20 μm and the error in the phase shift of the electron motion must not be greater than 2 degrees. The second reason is due to the technological evolution of the data acquisition and measurement control systems. During the recent years the interfacing standards followed an evolution in parallel with the computing devices.

The first approach was to provide a new choice for the moving equipment, in order to make it compatible with the new standards. For the scanning in the transverse plane the choice was to buy two continuous current linear stages with 200 mm of full range, capable to guarantee a high accuracy and repeatability smaller than one micron. The two motors are realised by Physik Instrumente (PI) and correspond to the M-521 DG model. The control of such devices, which are supplied with a linear encoder, is done with a closed-loop logic, by means of a PCI board placed into a PC-computer and controlled by proper PI drivers or, in alternative by software developed in a LabView environment. The maximum speed of such stages is 6 mm/s that allows simultaneous measurements of magnetic field and position. This technique has been used in ENEA by the FEL group that has developed an algorithm for fast scanning imaging acquisition.

For the longitudinal displacement an optical encoder is presently installed on the granite bar of the device, having a resolution of 10 μm, inadequate to the SPARC requirements and obviously to the SPARX project too. It is also installed a stepper motor interfaced with a RS232. This motor has been replaced with a new one from PI; is a continuous current motor with an optical encoder mounted, having a torque of 10 Ncm and 2000 counts per turn and its speed can be as high as 3 turns per second. Regarding the exact measurement of the longitudinal position of the magnetic probe different solutions have been analysed: the first is the substitution of the present optical encoder with a new one, but the only possibility to follow this way, with an appropriate guarantee is to forward the granite bar to the factory that would install the encoder. This hypothesis contains the risks of a double expedition of a very fragile item like a granite bar. The second solution considered is the use of laser interferometric system; such systems are now available on the market at reasonable prices (around 20 k€) and can be easily installed on any measurement device making them a multipurpose tool. In our case this system could also be used during the final alignment of the several undulator sections with the Linac and the transport channel. This is a very important and delicate task because the aim of the magnetic map measurements is to establish the magnetic axis position respect that of the mechanical one. The good alignment of all the magnetic axes of the undulator sections is crucial in order to let the electrons to follow a continuous trajectory and reach saturation in the SASE process with a higher efficiency.

As far as the magnetic measurements are concerned we should briefly provide the acquisition of a new Hall probe. The basic idea is to use a three axis probe in order to obtain the whole magnetic induction vector *B* with a single measurement. In order to evaluate the right dimension of the probe we have asked to the ACCEL company, in charge for the undulator realisation, to supply all the information about the probe they will utilise to measure and certify the magnetic structures. The importance of using similar equipments it is also related to all the formal obligations of goods acceptance.

The system for the data acquisition and control is based on PC computers and the LabView software fro National Instruments (NI). Such a combination has been already successfully tested in

ENEA for the control the FEL experiments. The two sources, the Compact-FEL and the CATS-FEL operate, since many years, with similar acquisition systems; such solution is so versatile that is currently used for many different applicative experiments. A series of developed codes will also be used, with all the proper modifications, for the SPARC project.

FEL Pulse Duration Measurements (2nd year)

The time scale of the radiation pulse in the SPARC SASE FEL process is extremely small, of the order of 3 ps r.m.s, and further smaller, few tens of femtoseconds, for the seeding experiment. It is thus impossible to measure the temporal pulse profile with conventional detectors which usually have time responsivity not much better than 1 ns. There are, however, some well known techniques with which it is possible to measure the time profile of short radiation pulses: the first method consists in using very fast electro-optical systems like Streak Camera. The second methods consist in using all optical techniques.

The first method is easier to apply, but it requires the use of a sophisticated and expensive instrumentation, moreover the best temporal resolution achieved in single shot is of the order of 1 ps. The second method is cheaper, but complex by the experimental point of view and requires information on the shape of the pulse. The advantage is the achievable resolution that can be as high as one femtosecond. Let us analyse the two techniques in detail.

The use of a streak camera has been considered because the FEL laboratory, in ENEA. The camera has been recently and refurbished by Hamamatsu using the EUROFEL project funds. The streak tube is the original one and it has only been tested by the company indicating resolutions very close to 1 ps. The new imaging unit is a CCD camera with optics down to 400 nm and a new software for the analysis of the images dispersed in time. Spontaneous emission measurements can be performed with this tool within the first phase of the SPARC project, for which the electron bunch length is of about 10 ps. Similarly Coherent Transition Radiation (CTR) or Cerenkov radiation can be measured for the evaluation of the electron beam profile. Together with these measurements the streak camera can be used for a statistical analysis of the time jitter between the electron beam and the gas-harmonic generated radiation in the seeding experiment in SPARC. The dynamical amplification process requires the necessity of synchronism between the seed and the electron bunch; this synchronisation could be problematic if the time jitter, related to the electron beam generation thread (Ti:Sa laser -> photo-cathode -> electron extraction ->acceleration) and to harmonic generation process (Ti:Sa laser -> gas jet), is longer than their time overlapping.

The measurement of the time jitter becomes complicated by the streak camera cannot operate in the repetitive regime because of the time structure of the SPARC source, the measurement must be performed in a single shot regime. In this regime the ENEA streak camera has an intrinsic trigger jitter of about 20 ps. To overcome these problems that limit the possibility of the single pulse jitter time evaluation, an experimental configuration has been proposed and it is reported in Fig.1.

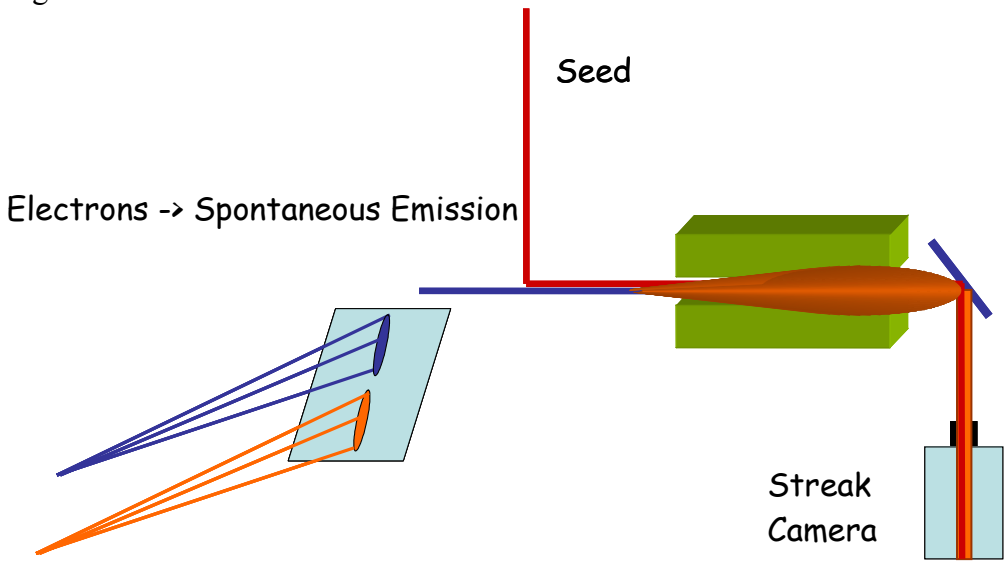

Fig.1 Experimental layout of the jitter measurement in the SPARC seeding experiment.

The two optical pulses under analysis are the spontaneous emission generated by the electrons and the seed itself. The two optical pulses can be separated in time by a proper amount in order to be captured by the screen of the Streak Camera, but still maintaining an appreciable distance. This can be done with a delay line on the seed trajectory. Due to the limited dynamic of the camera, the power level must be controlled attenuating the stronger of the two pulses. The streak camera start is then triggered by the first of the two optical pulses, this will ensure that, in spite of the trigger jitter that shifts the two images on the screen, the time separation of the two signals remains constant except for the quantity that can be ascribed to the relative jitter.

With the new software of the camera it is possible to analyse the data by measuring the distance of the maxima of the two spots, and then making a statistics after many shots.

The second method is based on autocorrelation measurements. The autocorrelation technique consists in creating a replica of the radiation pulse, let it pass through a variable delay line and then recombine both the pulses on a non linear device. The temporal overlapping of both the pulses is related to the amount of signal generated by the non linear process. With a proper variation of the optical delay it is possible to reconstruct the optical longitudinal profile.

The time measurements to be operated within the SPARC project present two main difficulties: a) due to the chaotic nature of the SASE mechanism any pulse shall have a different duration and thus any scanning technique cannot be applied; b) due to the wide spectral tunability of the source it will be necessary to find materials with non linear characteristics at wavelengths below 300 nm.

To solve the problems set by the point a) it is necessary to acquire an image in which any point correspond to a different delay Δt. To this purpose different geometries can be utilised that are generally based on an array or a matrix of non linear detectors capable to discriminate a response as a function of the spatial coordinate. In such a way it is possible to register, on different pixels of the matrix, different time delays. Making use of the parameters available on the market (matrices with spatial resolutions of about 10 μm, linear dimensions of few centimetres) it is possible to obtain temporal resolutions in the femtosecond range.

To solve the problems set by the point b) some particular materials can be used as crystals of BBO (Beta Barium Borate) or LBO (Lithium Borate), for which it have been established the possibility of use in autocorrelation experiments at wavelengths shorter τηαν 200 μm. Also crystals of MgF_2 are good candidate because they have a transparency window from 120 nm to 7 μm.